Direct production of cathode active material from black mass of spent lithium nickel manganese cobalt oxide batteries: Integrating and optimizing Li2CO3 recovery for

Resources, Conservation & Recycling Advances 28 (2025) 200291

Contents lists available at ScienceDirect

Resources, Conservation & Recycling Advances

journal homepage: www.sciencedirect.com/journal/Resources-Conservation-and-Recycling-Advances

Direct production of cathode active material from black mass of spent lithium nickel manganese cobalt oxide batteries: Integrating and optimizing Li_2CO_3 recovery for enhanced economic and environmental performance

Néstor Antuñano [a,*], Marlo Angelo Tito [a,b], Cristina Balza de Vallejo [a], Montserrat Galcerán [a], Martina Bruno [b], Silvia Fiore [b]

[a] Center for Cooperative Research on Alternative Energies (CIC energiGUNE), Basque Research and Technology Alliance (BRTA), Parque Tecnológico de Álava, 01510 Vitoria-Gasteiz, Spain

[b] DIATI, Department of Environment, Land and Infrastructure Engineering, Politecnico di Torino – Corso Duca degli Abruzzi, 24, 10129 Torino, Italy

ARTICLE INFO

Keywords:
Battery recycling
Lithium recovery
NMC cathodes
Circular economy

ABSTRACT

The growing demand for lithium-ion batteries (LIBs) highlights the need for efficient lithium recovery. Developing cost-effective, environmentally friendly extraction methods from secondary sources, such as end-of-life (EoL) Li-ion batteries, is essential for a sustainable lithium supply chain. This study optimizes Li_2CO_3 recovery, ensuring battery-grade quality, seamless integration into cathode active material (CAM) synthesis, and economic feasibility within hydrometallurgical recycling. Two approaches for single-stage Li recovery in a hydrometallurgical process with integrated CAM production from black mass of lithium nickel manganese cobalt oxide (NMC) LIBs are compared: homogeneous precipitation with Na_2CO_3 and heterogeneous precipitation using CO_2 gas. The analysis focuses on process efficiency, Li purity, and suitability for battery applications. Results show that selective CO_2-based precipitation demonstrated higher selectivity, achieving 97.10 % Li recovery (recoverable as Li_2CO_3), compared to 77.97 % for Na_2CO_3 precipitation, with both methods yielding battery-grade purity and morphology. Recycled NMC622 cathodes synthesized from recovered Li_2CO_3 achieved over 95 % of the discharge capacity of those from commercial Li_2CO_3. Recycled materials demonstrated excellent capacity retention and high coulombic efficiency (~100 %) after 30 cycles. Full-scale modeling assessed economic and environmental impacts in European LIBs recycling scenarios. Heterogeneous precipitation showed higher profitability (+0.73 M€/year) and greater net GHG reduction (986 t CO_2/year) but was more energy price-sensitive. Homogeneous precipitation demonstrated stable profitability (+0.62 M€/year); however, reduction in GHG emissions was more limited, reaching 518 t CO_2/year. This study integrates lithium recovery and water reclamation into a closed-loop process, enabling direct NMC cathode production, offering a sustainable and economically viable solution for LIBs manufacturing.

1. Introduction

The climate crisis underscores the urgent need for renewable energy, but the intermittent nature of renewable sources creates a supply-demand mismatch, which can be addressed through electrochemical energy storage. As a result, battery production is rapidly expanding, with lithium-ion batteries (LIBs) expected to dominate the market and reach up to 5500 GWh/year by 2040 (Degen et al., 2023). Among the various LIBs chemistries, NMC-based technologies are predicted to account for 50 % of this production by 2030 (Titirici et al., 2024). This increasing demand for LIBs leads to a rise in the extraction of critical materials like Li, Ni, Mn and Co, which are now listed as EU Critical Raw Materials (CRMs) due to economic and supply risks (Hool et al., 2023). Furthermore, the growing demand for LIBs leads to increased generation of hazardous waste at the end of their life, necessitating specialized treatment and contributing to overall waste accumulation (Gaines et al., 2023; Velázquez-Martínez et al., 2019; Melchor-Martínez et al., 2021; Mrozik et al., 2021). Thus, recycling LIBs significantly reduces the

* Corresponding author at: Center for Cooperative Research on Alternative Energies (CIC energiGUNE), Basque Research and Technology Alliance (BRTA), Parque Tecnológico de Álava, 01510 Vitoria-Gasteiz, Spain.
E-mail address: nantunano@cicenergigune.com (N. Antuñano).

https://doi.org/10.1016/j.rcradv.2025.200291

Available online 3 October 2025

carbon footprint of battery production by incorporating recycled materials into the synthesis of new active materials (Larouche et al., 2020; Latini et al., 2022).

State of the art LIBs recycling consists of pyrometallurgy and hydrometallurgy (Garole et al., 2020). Hydrometallurgical processes involve leaching followed by recovery steps to produce high-quality precursors for new LIBs, contributing to secondary raw materials supply as outlined by the European Battery Regulation (European Union, 2023). Battery recycling and materials recovery will not only be regulated (90 % for Ni and Co recovery and 50 % for Li by 2027 and 95 % for Ni and Co and 80 % for Li by 2031), but minimum mandatory levels of recycled content in new batteries will be set by 2030, with 15 % of cell materials required to come from recycling.

During leaching, target metals from LIB black mass are dissolved using mineral acids, organic acids, or alkaline solutions (Gao et al., 2018; Qing et al., 2023; Yu et al., 2023). Despite progress, further optimization of recovery rates and purity is needed to ensure a reliable LIB supply chain and cost-effective recycling (Jose et al., 2024; Marcinov et al., 2023). Li recovery remains challenging with current hydrometallurgical methods (Liu et al., 2019). Metals recovery for battery applications involves a complex sequence of leaching, purification, precipitation, and washing steps (Ramírez Velázquez et al., 2024), often resulting in material losses and impurities in the final Li-rich precipitates (Chang et al., 2025). Proven Li recovery methods—such as homogeneous precipitation with Na_2CO_3 and heterogeneous precipitation using CO_2—are widely applied to concentrated Li solutions (>10 *g*/L), typically achieving 85–97 % recovery (Gu et al., 2024; Zhao et al., 2019; Han et al., 2020; Raiguel et al., 2023; Aprilianto et al., 2024; Kim et al., 2024), but often fall short in delivering battery-grade purity (an insufficient 90–96 %) and morphology. Producing high-purity Li_2CO_3 requires additional, complex purification steps—such as selective impurity removal, fractional crystallization/reprecipitation, and ethanol or water washing—which increase Li losses and processing costs (Battaglia et al., 2022; Zhao et al., 2025; Gu et al., 2024; Joshi et al., 2024; Joshi et al., 2025).

This study develops, integrates, and optimizes a single-stage selective precipitation process (only precipitation and filtration) tailored for low-Li content liquors (<5 *g*/L) from black mass recycling (originating from the co-precipitation stage used for Ni, Mn, and Co precursor recovery), enabling the production of battery-grade Li_2CO_3 without additional steps. The recovered Li_2CO_3 is directly used in solid-state synthesis of NMC cathode materials, delivering electrochemical performance comparable to commercial standards. By eliminating multistep crystallization, purification and/or washing, this process simplifies operations and improves both economic and environmental outcomes, marking a significant step toward cost-effective, circular Li recovery from spent batteries.

Notably, all recovered materials, including Li_2CO_3, originate from the same hydrometallurgical recycling process, reinforcing a closed-loop and sustainable approach to battery material production. The novelty of this study lies in its lab-scale comparison of integrated homogeneous and heterogeneous precipitation methods, followed by the synthesis of NMC CAM using recycled precursors ($Ni_xMn_yCo_{1-x-y}(OH)_2$ and Li_2CO_3) from the same process, providing a comprehensive assessment of their technical and environmental impacts.

In this study, a lithium recovery step is integrated into the process to enable circular CAM production from spent NMC batteries. The selective precipitation of battery-grade Li_2CO_3—suitable for solid-state synthesis of recycled NMC—is investigated, optimized, and evaluated from technical, economic, and environmental perspectives. This Li recovery stage is the final step in a battery recycling process (Fig. 1) that includes: (1) dissolving the black mass of EoL NMC LIBs using sulfuric acid (H_2SO_4) and hydrogen peroxide (H_2O_2) to extract metal ions (Mn^{2+}, Co^{2+}, Ni^{2+}, Li^+, and other impurities) from graphite; (2) purifying the leachate to remove Fe, Al, and Cu with minimal loss of target elements; and (3) a co-precipitation step to produce the NMC precursor, $Ni_xMn_yCO_{1-x-y}(OH)_2$, under a nitrogen atmosphere with controlled stoichiometry. The co-precipitation step was optimized to achieve recovery efficiencies of 99.9 % for Ni, 97.9 % for Mn, and 99.7 % for Co, while only 6.9 % of Li was co-precipitated, with the majority remaining in solution. Efficient recovery of residual Li—considering yield, purity, and morphology—is essential for integrating CAM production into the recycling process. This step is key to establishing a sustainable, economically viable pathway for EoL battery recycling and enabling true circularity in the battery value chain.

This study examines the integration of an optimized Li recovery stage for the remaining Li-bearing solution, ensuring the production of Li_2CO_3 suitable for direct NMC CAM synthesis and validating its use in new

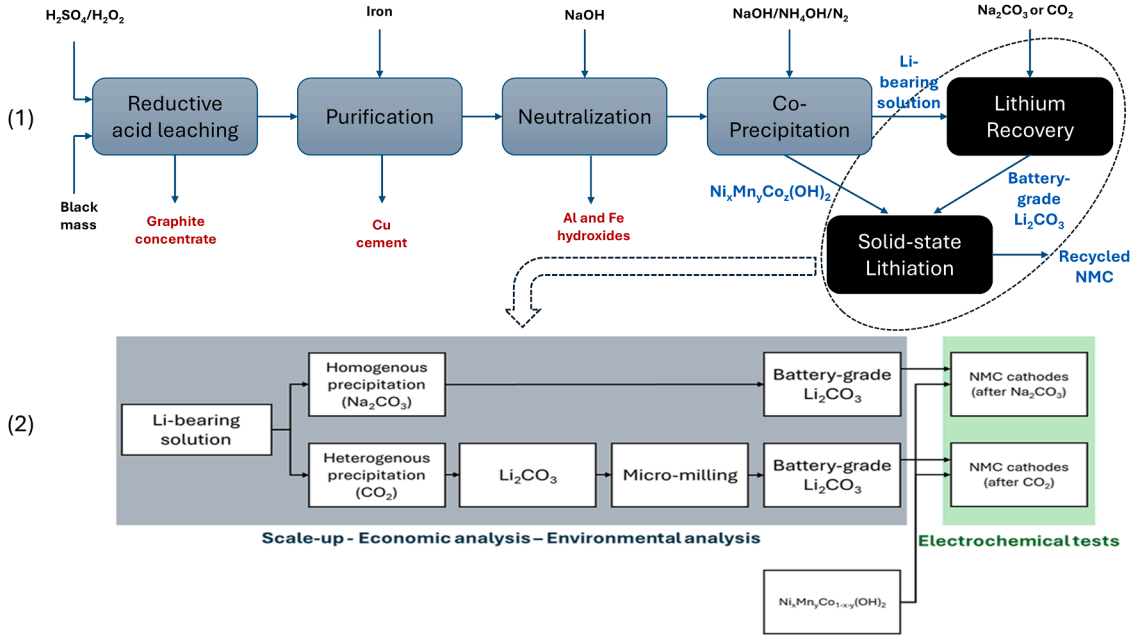

Fig. 1. (1) Flowsheet of the hydrometallurgical recycling process with integrated CAM synthesis from black mass of EoL NMC LIBs. The studied, optimized, and evaluated part of the process is shown in black. (2) Concept of this study.

electrode fabrication. This supports a closed-loop recycling process that enables CAM production directly from black mass.

A model of the integrated Li recovery stage was also developed to simulate homogeneous and heterogeneous precipitation at full scale, assessing the scalability, economic viability, and environmental impact of both methods in the context of Li recovery from battery recycling in Europe. The overall conceptual framework of the study is illustrated in Fig. 1.

2. Materials and methods

2.1. Li_2CO_3 recovery: homogenous and heterogenous precipitation

The solution fed to the Li recovery stage is the filtrate from the co-precipitation process, simulated using a stock solution representative of LIB black mass hydrometallurgical recycling after leaching and purification steps that recover Li, Co, Ni, and Mn while removing Al, Fe, and Cu. The following reagents were used: lithium sulfate monohydrate (>99.0 %), nickel sulfate hexahydrate (≥99.0 %), manganese sulfate monohydrate (≥99.0 %), and cobalt sulfate heptahydrate (≥98.0 %), all from ThermoScientific. Sodium sulfate anhydrous (≥99.0 %), sodium hydroxide (4 M), and ammonium hydroxide (5 M) were supplied by Honeywell–Fluka. This simulated liquor was used in the optimized co-precipitation stage to maximize Ni, Mn, and Co recovery, forming solid $Ni_xMn_yCo_{1-x-y}$ and a Li-bearing filtrate. The process was conducted at pH 11 (adjusted using 3 M NaOH and 0.15 M NH_4OH) and maintained at 50 °C for 60 min. Two recovery methods were tested to precipitate Li_2CO_3 from Li-bearing filtrate: homogenous precipitation by adding Na_2CO_3 (≥ 99.8 % Honeywell–Fluka) and heterogenous precipitation via CO_2 flow (CO_2 extra-pure Nippon Gases, 40 bar). All experiments involving Ni, Mn, and co-precipitation, as well as Li recovery, were conducted in a 1 L glass reactor equipped with mechanical stirring and gas injection, operated within a thermostatic bath. A ThermoScientific Orion Star A111 multiparameter instrument was used to monitor and control pH and temperature. Several operational parameters were tested during the precipitation experiments, including durations of 0.25, 0.5, 1, and 2 h; temperatures of 50 °C, 70 °C, and 90 °C; and stoichiometric ratios of Li+ to Na_2CO_3 of 1:1.1, 1:1.2, and 1:2 for homogenous. Similarly, several parameters were tested during heterogenous precipitation, including durations of 1, 2 and 3 h; temperatures of 70 °C, and 90 °C; and CO_2 gas flow of 100 mL/min, 150 mL/min and 200 mL/min. These gas flow rates correspond to Q_G/V_L ratios of 1.22 s^{-1}, 1.83 s^{-1} and 2.44 s^{-1}, respectively, for the batch stirred tank reactor, where Q_G is the gas flow rate (m^3/s) and V_L is liquid volume in the reactor (m^3). NaOH was added during heterogenous precipitation to control the solution pH. Liquid and solid samples were collected for analysis and characterization following filtration with a Millipore ASME-MU high-pressure filter. The filters containing solid samples from $Ni_xMn_yCo_{1-x-y}(OH)_2$ precursor co-precipitation stage were washed with distilled water before drying, whereas the recovered Li precursors were directly placed in a drying oven at 105 °C. Micro-milling tests of Li_2CO_3 precipitated using CO_2 were conducted with a Fritsch Planetary Micro Mill Pulverisette 7, equipped with a zirconia grinding bowl (45 mm diameter) and balls (7 mm diameter). The milling process was carried out at a 40 % load rate and a rotational speed of 290 rpm.

The two recovery methods were compared based on the yield of Li recovery and the purity of the recovered Li_2CO_3, see Eq. (1) and Eq. (2), where, $V_{o,\ liquor}$ and $V_{f,\ filtrate}$ represent the initial and final liquid volumes (in L) before and after Li_2CO_3 precipitation, respectively. $[Li^+]_o$ and $[Li^+]_f$ are initial and final Li concentration in the liquid (in g/L), respectively. Then $\%Na_{Li2CO3}$ is the sodium concentration in the Li_2CO_3 produced (expressed on a per unit basis) and MM_{Na} and $MM_{Na\ impurity}$ refer to the molecular weights (in g/mol) of sodium and the identified sodium-based crystalline impurity, as determined by XRD analysis.

$$Recovery\ (\%\ Li) = \left[1 - \frac{V_{f,filtrate} \mathrm{x} [Li^+]_f}{V_{o,filtrate} \mathrm{x} [Li^+]o}\right] \mathrm{x}\ 100 \quad (1)$$

$$Purity\ (\%\ Li2CO3) = \left[1 - \frac{MM_{Na\ impurity} \mathrm{x} \%Na_{Li2CO3}}{2MM_{Na}}\right] \mathrm{x}\ 100 \quad (2)$$

2.2. Analytical methods

The chemical composition of liquid streams was analyzed by ICP-OES (Agilent-5800) after collecting and acidifying aliquots with 2 % v/v HNO_3 to stabilize metal ions and prevent losses. Samples were diluted with deionized water to fit the calibration range. Calibration used certified multi-element standards with Ga as an internal standard to correct for matrix effects and drift. Solid samples (≈25 mg) were digested in 10 mL concentrated HNO_3 using a Milestone ETHOS-UP microwave digestion system and analyzed by ICP-OES. Total sulfur content was measured using a LECO S-632 elemental analyzer. The crystalline structure of the solid samples was identified through X-ray powder diffraction (XRD) analysis with a Bruker D8 Advance Diffractometer in Bragg-Brentano geometry (θ-θ) using $CuK_{a1,2}$ radiation. Additionally, Le Bail refinements were performed using the FullProf Suite (Rodriguez-Carvajal, 1993) to obtain the unit cell parameters. The morphology of the samples was analyzed using Scanning Electron Microscopy (SEM) with a Quanta FEG-250 microscope operated at 30 kV, equipped with an Apollo 10 SSD energy-dispersive X-ray spectrometer (EDS). The particle size distribution (PSD) of the materials was determined using a Laser Diffraction Analyzer (Malvern Panalytical Mastersizer-3000).

2.3. Electrochemical testing of recycled cathode material

The Li_2CO_3 recovered both after homogenous and heterogenous precipitation was mixed with $Ni_xMn_yCo_{1-x-y}(OH)_2$ samples from co-precipitation stage using a roller mixer (Stuart SRT6D) at a stoichiometric ratio of 1:2 (Eq. (19)). The mixture was then thermally treated at 500 °C for 6 h, followed by calcination at 850 °C for 12 h in a Carbolite Gero CWF-1200 furnace under an air atmosphere. These synthesized NMC cathode materials obtained from recovered Li_2CO_3 were electrochemically benchmarked against NMC synthesized using commercial battery-grade Li_2CO_3 (≥99.0 % purity, Thermoscientific) as the Li precursor. The active material NCM was mixed with C65 carbon additive (Imerys) and Polyvinylidene fluoride (PVDF-Solvay) binder in a mass ratio of 85.0:7.5:7.5 N-methyl pyrrolidinone (NMP–Sigma-Aldrich). Then, the slurry was cast on an aluminium current collector and dried overnight at 120 °C under vacuum. Half cells were assembled using Whatman GF/D borosilicate glass, a 1.0 M solution of LiPF6 in 1:1 vol. EC:DMC (LP30–Sigma-Aldrich) and high purity Li metal as a separator, electrolyte and negative electrode, respectively. The cells were charged and discharged in the galvanostatic mode at C/20 in the voltage range 2.7–4.3 V vs. Li^+/Li.

2.4. Process scale-up

The process of Li_2CO_3 recovery was scaled up considering a plant with a treatment capacity of 2500 t/y of black mass, which is considered a representative treatment capacity for LIBs recycling plants (Bruno and Fiore, 2024). Energy and materials flows were estimated based on the optimal operative conditions identified from the experimental set up were taken into consideration for the scale up of the Li recovery process by the two considered scenarios: recovery of Li_2CO_3 by homogenous precipitation with Na_2CO_3 (Scenario 1) and by heterogenous precipitation via CO_2 flow (Scenario 2). The boundaries of the system and the materials and energy flows are shown in Appendix A Figure A1-A2-A3. The scale-up methodology for each step of the Li_2CO_3 recovery process is detailed in the Appendix A Section A1. The design methodology was

developed and simulated using computing software MATLAB® version: 9.13.0 (R2022b).

2.5. Economic analysis

The economic feasibility of the two proposed scenarios was assessed through cash flow (C_t), net present value (NPV), return of investment (ROI) and payback time. Cash flow (C_t), was calculated by subtracting the operative costs (OPEX) from revenues from Li_2CO_3 sales (R), the see Eq. (3). NPV was calculated as the difference between the capital investment (C_0) and the cumulative discounted cash flows considering a discount rate (i) of 10 % over each year (n), see Eq. (4). ROI was calculated as the ratio between the NPV and the C_0, see Eq. (5), and the payback time can be identified as the first year with ROI > 0.

$$C_t(mln \in /y) = R - OPEX \quad \text{(Eq. 3)}$$

$$NPV(mln \in /y) = -C_0 + \sum_{n=1}^{N} \frac{C_t}{(1+i)^n} \quad \text{(Eq. 4)}$$

$$ROI\ (\%) = \frac{NPV}{C_0} \quad \text{(Eq. 5)}$$

Revenues were based on the current market price of Li_2CO_3 (9966.75 €/t). OPEX included the costs for black mass (300 €/t), chemical reagents (Ecoinvent, 2024), electricity (Eurostat, 2024a), gas (Eurostat, 2024b), waste treatment (European Environmental Agency, 2023), labour costs (Eurostat, 2024c) and equipment maintenance. The operational basis of the process is based on the optimal duration of the Li recovery process, as determined by experimental results, and considered a working time of 2096 h/y for Scenario 1, corresponding to 8 batch/d over 262 d/y, and 3144 h/y for Scenario 2, corresponding to 4 batch/d over 262 d/y. Maintenance costs were assumed to be 5 % of the C_0, which included the cost of purchasing the equipment and the costs of pipes (60 % of equipment cost), electrical connections (11 %) and building infrastructure (18 %), which are typical for chemical plants (Chemical Engineering Projects, 2014). Equipment costs were estimated according to literature (Loh et al., 2002), and adjusted for inflation (US Inflation Calculator, 2025), see Appendix A Table A1. Both scenarios were assumed to be potentially implemented in an existing LIBs recycling plant, with overhead costs such as land, storage, office space, and administrative labor allocated outside the system boundaries of this economic analysis.

A sensitivity analysis on profitability was performed considering location-based factors (electricity, labour, waste disposal) for eight European countries (Denmark, Finland, Germany, Italy, Poland, Romania, Spain, Sweden) and market fluctuations (Li_2CO_3 prices) over a 10-year period (2016–2025) (Benchmark Mineral Intelligence, 2025).

2.6. Environmental analysis

The environmental analysis performed in this study is based on the net balance between the GHG emissions generated by the recycling process and the GHG emissions avoided, by recycling of Li_2CO_3 from LIBs black mass, instead of from primary mineral extraction. The GHG emissions generated by the recycling process were calculated based on the GHG emissions index of electricity and natural gas production, chemical reagents manufacturing and hazardous waste management (Ecoinvent, 2024; European Environment Agency, 2024). Eventually, the GHGs emissions associated with the extraction of primary Li minerals were considered a negative factor in the overall GHG emissions balance, since recycling replaces the need for mining activities.

3. Results and discussion

3.1. Li_2CO_3 recovery

In this study, the Li recovery stage through the selective precipitation of Li_2CO_3 was investigated and optimized as a critical step in a hydrometallurgical recycling process with integrated CAM synthesis for EoL NMC LIBs. To this end, the effects of the selected precipitating agent, reagent dosage, temperature, and reaction time were analyzed, not only in terms of techno-economic feasibility, focusing on maximizing the recovery yield of a battery-grade Li precursor to produce recycled NMC active material, but also in relation to the environmental impact of the process. The Li_2CO_3 precipitation reaction from the exhausted liquor of the Ni, Mn and Co precursor coprecipitation step (Table 1) has been developed, optimized and evaluated by adding Na_2CO_3 or bubbling CO_2 (g) as precipitating agent. Homogenous and heterogenous selective precipitation of Li_2CO_3 were studied under varying conditions.

The effect of operating conditions—especially the choice of precipitating agent (Na_2CO_3 or CO_2 gas)—was studied to understand their influence on chemical equilibria, including solubility, acid-base, and gas–liquid interactions, as well as their impact on nucleation and crystal growth. The analysis offers mechanistic insights into the thermodynamic and kinetic factors influencing Li_2CO_3 recovery efficiency, purity, and morphology under various conditions.

$$CO_2\ (aq) + OH^- \leftrightarrow HCO_3^-\ K_1\ (T) \quad \text{(Eq. 6)}$$

$$HCO_3^- + OH^- \leftrightarrow CO_3^{2-} + H_2O\ K_2\ (T) \quad \text{(Eq. 7)}$$

$$NH_4^+ + OH^- \leftrightarrow NH_3\ (aq) + H_2O\ K_3\ (T) \quad \text{(Eq. 8)}$$

$$NH_3\ (aq) + HCO_3^- \leftrightarrow NH_2COO^- + H_2O\ K_4\ (T) \quad \text{(Eq. 9)}$$

$$H_2O \leftrightarrow H^+ + OH^-\ K_w\ (T) \quad \text{(Eq. 10)}$$

$$Li^+ + HCO_3^- \leftrightarrow LiHCO_3\ (s)\ K_{ps1}\ (T) \quad \text{(Eq. 11)}$$

$$2\ Li^+ + CO_3^{2-} \leftrightarrow Li_2CO_3 \downarrow (s)\ K_{ps2}\ (T) \quad \text{(Eq. 12)}$$

Homogenous precipitation:

$$Na_2CO_3\ (s) \leftrightarrow 2\ Na^+ + CO_3^{2-}\ K_{ps3}\ (T) \quad \text{(Eq. 13)}$$

Heterogenous precipitation:

$$CO_2\ (g) + H_2O \leftrightarrow CO_2\ (aq)\ h_{CO2}\ (T) \quad \text{(Eq. 14)}$$

During heterogenous precipitation, the concentration of carbonate ion ($[CO_3^{2-}]$) in the system depends on the gas-liquid transfer rate of CO_2 (F_{CO_2}) in the reactor (Eq. (15)) (Wylock, C. et al., 2014).

$$F_{CO_2} = -\frac{A_{GL}}{V_L} K_G \left(p_{co_2 g} - p^*_{co_2}\right) \quad \text{(Eq. 15)}$$

Where:

K_G = Mass transfer coefficient (mol/m^2.s)

$p_{co_2 g}$ = Partial pressure of CO_2 in bulk gas flow (Pa)

$p^*_{co_2}$ = Equilibrium partial pressure of CO_2 (Pa)

A_{GL}= Total gas-liquid interfacial area (m^2)

V_L = Volume of liquid in the reactor (m^3)

The morphology of the recovered Li_2CO_3, mainly characteristic crystal size (L), is crucial not only for precipitation and solid-liquid separation yields but also for its suitability in battery applications.

Table 1
Composition of filtrate after co-precipitation stage, feed solution of studied Li recovery stage.

pH	$[Li^+]$ (g/L)	$[Na^+]$ (g/L)	$[SO_4^{2-}]$ (g/L)	$[NH_3]$ (g/L)	$[Ni^{2+}]+[Mn^{2+}]+[Co^{2+}]$ (mg/L)
11.3	4.34	25.91	88.99	4.86	0.56

Optimizing crystal growth mechanisms and kinetics (Lewis et al., 2015) is vital to enhance the effectiveness of this selective precipitation step (Eq. (16) and 17).

$$G = \frac{dL}{dt} = k_{g,o} e^{\frac{-E_{act}}{RT}} (C - C_{sat})^{g} (24)\ n(L) = n_o e^{\left(-\frac{L}{Gt}\right)} \quad \text{(Eq. 16)}$$

Where:

G = Crystal growth rate. The increase in crystal size due to deposition of solute on crystal surface (m.s^{-1})

t = Residence time (s)

ΔC = Supersaturation (mol.m^{-3}) k_g = Growth rate constant (m.s^{-1})

g = Order of the growth rate (-) n (L) = Population density of crystals (number of crystals.m^{-3}) n_o = Population density of nuclei (number of nuclei.m^{-3})

Since supersaturation is the thermodynamic driving force for crystal size, precipitation parameters must be optimized to control its deviation from equilibrium (Eq. (6) to 14):

$$\Delta C = \frac{\gamma_{Li^+}[Li^+]\gamma_{CO_3^{2-}}[CO_3^{2-}] - K_{ps2}(T)}{K_{ps2}(T)} = \frac{[\text{Li2CO3}] - [\text{Li2CO3}]\text{sat}}{[\text{Li2CO3}]\text{sat}} \quad \text{(Eq. 17)}$$

For the homogeneous precipitation alternative, the effect of process temperature, duration and Na_2CO_3 dosage on the recovery rate of Li and purity of the recovered Li_2CO_3 were studied (Fig. 2). Results confirmed that higher temperatures reduced Li solubility, promoting precipitation, see Appendix B, Figure B1. While longer reaction times improved Li recovery rate, duration exceeding 1 hour decreased Li_2CO_3 purity due to the formation of sodium salts as side products. Similarly, higher stoichiometry ratio of Li^+ to Na_2CO_3 (Eq. (12) and 13) improved the recovery yield but compromised purity of the recovered Li_2CO_3. The optimal conditions for Li_2CO_3 recovery via homogeneous precipitation were determined to be a 1-hour reaction at 90 °C with a stirring speed of 600 rpm and a Na_2CO_3 stoichiometric addition factor of 1.2. Under these conditions, the highest Li_2CO_3 recovery yield was achieved, corresponding to 51.5 % of the Li feed, with a purity exceeding 97.0 %. Given that the solubility of Li_2CO_3 at 90 °C is 7.9 g/L (Appendix B, Figure B1), this optimized recovery process with Na_2CO_3 maximizes Li extraction while ensuring a purity level suitable for battery applications (≥ 97.0 %), representing 77.97 % of the recoverable Li as carbonate through selective precipitation. In this way, the integrated stage completes the hydrometallurgical recycling process, achieving a total Li recovery of 58.1 %.

In the case of heterogeneous precipitation, the effect of temperature, reaction time, and CO_2 injection rate on the production of Li_2CO_3 from co-precipitation filtrate was analysed to optimize recovery and purity (Fig. 2). During heterogenous precipitation, CO_2 absorption acidifies the solution (Fig. 2), leading to the formation of undesirable bicarbonates as the dominant species at pH levels below 10.3 (Han et al., 2020). Therefore, precise pH control is crucial for facilitating Li_2CO_3 precipitation, preventing the formation of soluble $LiHCO_3$, and minimizing the need for pH modification with NaOH due to the buffering effect of the carbonates system *(Appendix B, Table B1)*. Simultaneously, increasing the process temperature reduces CO_2 dissolution (affecting the pH gradient) and lowers its transfer rate to the liquid, despite improving reaction kinetics, creating a trade-off in process optimization. Furthermore, increasing the CO_2 flow rate was limited at optimal absorption efficiency (Eq. (15)) due to the balance between reduced bubble size and shortened bubble retention time. The highest Li_2CO_3 recovery yield, 64.2 % of the Li feed, with a purity exceeding 97.0 %, was achieved under optimized conditions of 90 °C, a stirring speed of 700 rpm, and a CO_2 injection rate of 200 mL/min for 3 h. Under these conditions, 97.1 % of the recoverable Li as Li_2CO_3 was successfully precipitated, contributing to a closed-loop hydrometallurgical process with a total Li recovery of 70.9 %.

As shown in Fig. 3, all Li_2CO_3 materials recovered through homogeneous and heterogeneous precipitation crystallize in the characteristic monoclinic structure with space group *C2/c*, consistent with the Li_2CO_3 commercial material and the Bragg positions from the database. Differences in the peak profiles can be observed, primarily attributed to variations in particle shape and size, as clearly shown in the SEM images (Fig. 3). Notably, in the Li_2CO_3 obtained through selective precipitation

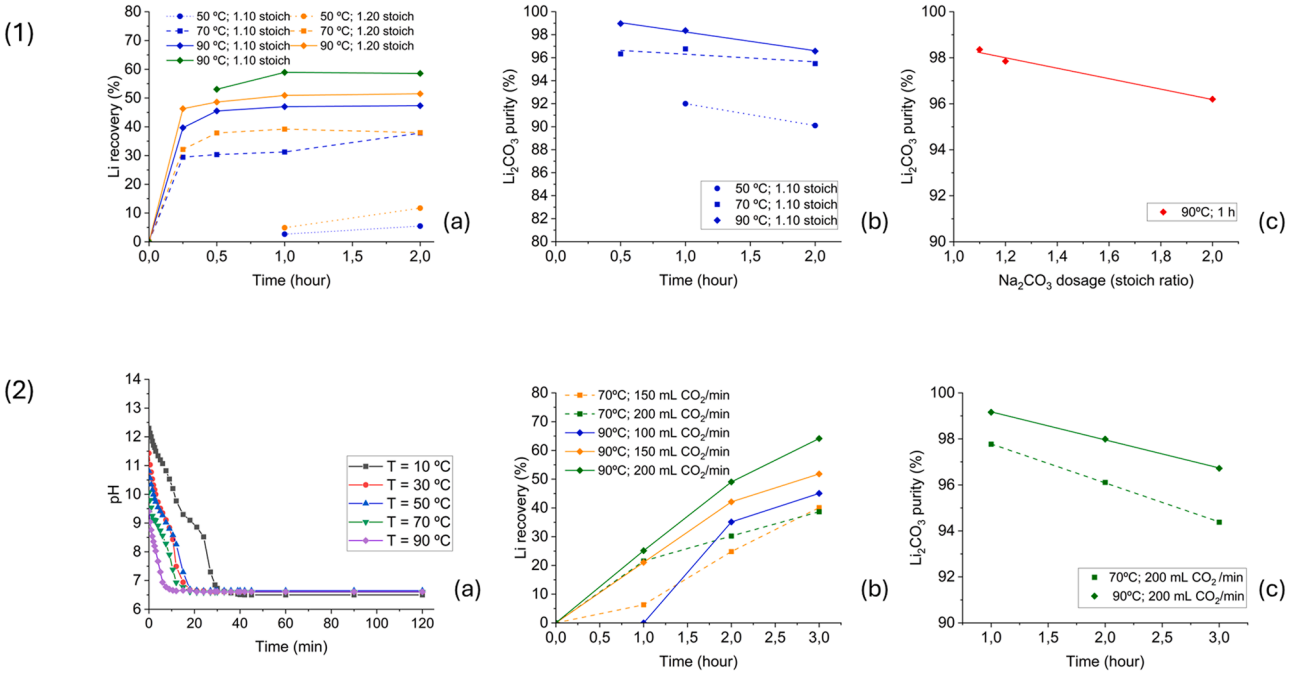

Fig. 2. Kinetic and Thermodynamic study of Li_2CO_3 selective precipitation. (1) Homogeneous precipitation: (a) Effect of temperature, Na_2CO_3 stoichiometric ratio, and reaction time on Li recovery rate; (b) effect of temperature and reaction time on Li_2CO_3 purity; (c) effect of Na_2CO_3 stoichiometric ratio on Li_2CO_3 purity during homogenous precipitation. (2) Heterogenous precipitation: (a) Effect of co-precipitation filtrate temperature on pH evolution over time during CO_2 bubbling (200 mL CO_2/min at 700 rpm); (b) effect of temperature, CO_2 flow rate and reaction time on Li recovery rate and (c) effect on Li_2CO_3 purity.

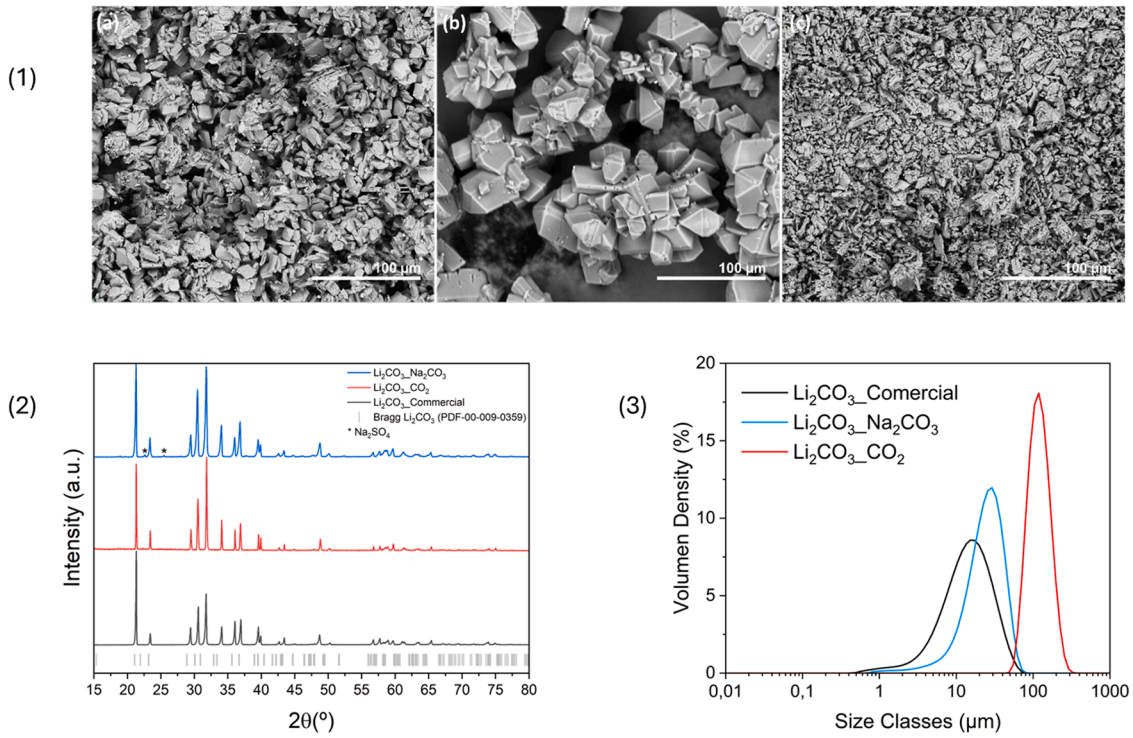

Fig. 3. Morphological and structural characterization of recycled Li_2CO_3 samples. (1) SEM images of (a) the optimized product from homogenous precipitation, Li_2CO_3 recycled by adding Na_2CO_3, (b) the optimized product from heterogeneous precipitation, Li_2CO_3 recycled by bubbling CO_2 and (c) commercial battery-grade Li_2CO_3. (2) XRD patterns of the recycled Li_2CO_3 by different methodologies compared with the commercial one. The grey lines show the Bragg position of the Li_2CO_3 from database. (3) Particle-size distribution of Li precursors used in the CAM synthesis stage: commercial Li_2CO_3 (blue), Li_2CO_3 precipitated using Na_2CO_3 (green) and Li_2CO_3 bubbling CO_2 (red).

with Na_2CO_3, minor peaks corresponding to Na_2SO_4 can be detected, aligning with the measured purity of the product (Eq. 2). The unit cell parameters obtained through LeBail refinement (Appendix C, Table C1 and Figure C1) show good agreement with the literature values (Idemoto et al., 1997).

Beyond impurity control in Li precursors, particle size distribution and morphology are critical factors in determining the suitability of Li_2CO_3 for CAM synthesis. The influence of optimized reaction variables on the crystallization mechanism was evaluated, revealing distinct differences between the two precipitation methods. In homogeneous precipitation, the recovered product exhibited fine crystal agglomeration with a median particle size (d_{50}) of 26.4 µm. In contrast, heterogeneous precipitation led to the formation of significantly larger agglomerates, with a median particle size of 120 µm (Fig. 3).

Morphological differences, influenced by the residence time in the stirred-tank reactor (Eq.18), are crucial for achieving Li_2CO_3 with the required quality for battery applications.

$$L_{50} = 3,67(Gt) \quad \text{(Eq. 18)}$$

Chemical adsorption and reaction kinetics play a crucial role in determining the average crystal size (L_{50}), influenced by the crystal growth rate, and subsequently affect the agglomeration mechanism (Franke and Mersmann, 1995). In addition, as described in Eq. (19), the collision frequency kernel (β) is adjusted for turbulent flow conditions (Lewis et al., 2015), helping to explain the greater tendency for agglomeration observed during heterogeneous precipitation (Fig. 3). This behavior is attributed to the larger average crystal size, which directly influences the agglomeration mechanism under the specific conditions of Li recovery.

$$\beta(L_i, L_j) = \frac{4}{3}\sqrt{\varepsilon/\nu}(L_i + L_j)^3 \quad \text{(Eq. 19)}$$

where:

L_i and L_j crystal size of two crystals (m)

ε = Mean energy dissipation rate ($W.kg^{-1}$)

ν = Kinematic viscosity ($m^2.s^{-1}$)

3.2. Wastewater reclamation

In both precipitation options, after maximizing the recovery of battery-grade Li_2CO_3, a Li-containing alkaline solution (pH= 10.3 – 11.0 and high concentrations of sodium, sulphate and carbonate ions) remains as a residual stream of the hydrometallurgical process. A conventional chemical treatment process that relies on precipitation reactions has been designed in order to reduce [SO_4^{2-}] and [CO_3^{2-}], reusing the solution obtained as a reagent in the neutralization stage of the hydrometallurgical recycling process with integrated CAM synthesis (Fig. 1). When calcium hydroxide is added to the exhausted liquor at 20 °C, 600 rpm and controlled pH between 12.0 – 12.5, it reacts to form calcium sulfate ($CaSO_4$) and calcium carbonate ($CaCO_3$), which have low solubility in water and precipitates out (Eq. (20)).

$$Ca(OH)_2\,(aq) + SO_4^{2} + CO_3^{2-} + Na^+ + Li^+ \leftrightarrow CaSO4\downarrow\,(s) + CaCO3\downarrow\,(s) + 2OH^- + Na^+ + Li^+ \quad \text{(Eq. 20)}$$

The optimal $Ca(OH)_2$ dosage for wastewater reclamation in the hydrometallurgical process was determined under the cited operating variables for 45 min, achieving a constant [SO_4^{2-}]+[CO_3^{2-}] concentration below 1,55 g/L with less than 2 % of Li losses, ensuring its recirculation.

This liquor regeneration step enables efficient wastewater treatment while retaining Li in the system. It lowers chemical use, especially alkaline solutions for pH adjustment during neutralization, and promotes gradual Li concentration for later recovery. This approach supports a zero-waste process, enhancing the sustainability of EoL battery recycling.

3.3. Synthesis of recycled NMC active material with recovered Li_2CO_3

Recycled NMC is obtained through solid-state lithiation at elevated temperatures, utilizing previously co-precipitated Ni, Co, and Mn hydroxides (Table 2) in combination with recovered Li_2CO_3 (Table 3), both derived from the hydrometallurgical recycling process, under an air atmosphere (Eq. (21)).

$$\tfrac{1}{2}\,Li_2CO_3\,(s) + Ni_xMn_yCo_{1-x-y}(OH)_2\,(s) + 4/3\,O_2\,(g) \leftrightarrow Li(Ni_xMn_yCo_{1-x-y})O_2\,(s) + CO_2\,(g) + H_2O\,(g) \quad \text{(Eq. 21)}$$

As shown in Fig. 4, the main peaks in the XRD patterns of NMC_Li_2CO_3_commercial and NMC_Li_2CO_3_Na_2CO_3 correspond to the characteristic NMC phase, assigned to the *R*-3*m* space group. In contrast, the XRD pattern of NMC_Li_2CO_3_CO_2 exhibits a noticeable splitting of the main peaks, suggesting the presence of two distinct NMC phases with differing composition. These results suggest that the physicochemical properties and characteristics of Li_2CO_3 used as a precursor play a crucial role in determining the structure and characteristics of the synthesized NMC. Additionally, minor peaks associated with unidentified impurities are observed in the XRD patterns. However, these impurities do not significantly affect the structural integrity of the final NMC622 compounds. Their presence could potentially be mitigated through optimization of the synthesis conditions. The cell parameters of the NMC samples determined through Le Bail refinement (Figure S2 and Table S2) show good agreement with previously reported values in the literature (Tahmasebi and Obrovac, 2024). Furthermore, both NMC_Li_2CO_3_Commercial and NMC_Li_2CO_3_Na_2CO_3 exhibit comparable crystallite sizes, correlating with the characteristics of the Li precursors used in their synthesis (Fig. 3 and Table 3).

The characterization of the synthesized products reveals the influence of Li_2CO_3 morphology (Fig. 3) on the synthesis reaction and the resulting CAM properties (Fig. 4). This morphology is primarily governed by the crystallization and agglomeration mechanisms during the precipitation stage. The NMC synthesized using Li_2CO_3 obtained under the optimized operating conditions of homogeneous precipitation exhibits similar morphology, particle size distribution, and shape (Fig. 4) to that obtained from commercial battery-grade Li_2CO_3. However, deviations in these properties were observed when Li precursors from heterogeneous precipitation were used. This discrepancy suggests that factors beyond chemical purity, as both scenarios produced Li_2CO_3 with comparable composition, may play a significant role in the NMC synthesis process. Specifically, variations in physical characteristics such as particle size and surface area of Li_2CO_3 recovered under heterogeneous precipitation appear to impact the reaction dynamics. In this case, the morphology resulting from the precipitation-crystallization conditions when CO_2 is used can be modified and optimized through additional recrystallization or a controlled ball milling step, making the obtained Li_2CO_3 suitable for commercial CAM production. In this context, ceramic ball milling has been identified as an efficient method for the industrial-scale micronization of recovered Li_2CO_3, enabling the transition from the d_{80}=158 μm of Li_2CO_3 produced by CO_2-optimized selective precipitation to the d_{80}=36.6 μm required for suitable NMC synthesis. This process is effective, provided that proper process controls and appropriate milling media are used to ensure optimal quality and efficiency.

These findings underscore the potential of the optimized recovery process to obtain Li precursors for producing recycled NMC CAM with properties comparable to those from conventional sources, reinforcing the feasibility of integrating recycled materials into battery manufacturing.

Table 3
Chemical composition of Li precursors obtained through optimized homogeneous and heterogeneous precipitation.

Sample	Li_2CO_3 (%)	Na (%)	S (%)	Ni (ppm)	Mn (ppm)	Co (ppm)
Li_2CO_3 using Na_2CO_3	97.1	0.94	0.64	107	44	34
Li_2CO_3 bubbling CO_2	96.9	1.07	0.70	107	44	17

3.4. Electrochemical performance of recycled CAM

The cycling performance and coulombic efficiency of recycled NMC622 cathodes synthesized using two different Li_2CO_3 precursors, commercial-grade Li_2CO_3 and Li_2CO_3 recovered in precipitated with Na_2CO_3, are shown in Fig. 5. While the cathode using commercial Li_2CO_3 exhibits a slightly higher initial discharge capacity (155 $mAh.g^{-1}$ vs. 136 $mAh.g^{-1}$), both materials demonstrate stable cycling performance with coulombic efficiencies approaching 100 %. As is typical for NMC materials, an initial formation step is required to stabilize the layered structure, explaining the progressive increase in capacity observed during the early cycles. The ~3 % difference in maximum discharge capacity after formation is attributed to the presence of non-active Na_2SO_4 impurities in the recovered precursor, which remain inert under the oxidizing conditions used during solid-state lithiation. Notably, the CAM synthesized with recovered Li_2CO_3 shows comparable long-term electrochemical performance and excellent capacity retention, indicating that ≥97.0 % purity is sufficient for high functionality. These results confirm the potential of recovered Li precursors for fully recycled CAM and highlight the need to optimize Li recovery to balance purity, morphology, structure, and electrochemical performance.

3.5. Material flow and process scale up

The materials and energy flow were calculated for a full-scale recycling facility with a processing capacity of 2500 t/y of black mass, where 12,750 m^3/y of Li-bearing solution undergoes Li recovery. In the case of scenario 1596 t/y of Na_2CO_3 are required to precipitate 203 t/y of Li_2CO_3. Whereas, in Scenario 2, 1517 t/y of CO_2 are required to precipitate 256 t/y of Li_2CO_3 and 4054 m^3/y of pH buffer solution, containing 2 t/y of NaOH are also necessary to stabilize the solution pH and enable Li_2CO_3 precipitation. The presence of a buffer solution increases the amount of wastewater produced by the press filter to 13,994 m^3/y, rather than the 10,618 m^3/y of wastewater filtered out in Scenario 1. In both scenarios, after filter press the generated wastewater is recovered by adding 1500 t/y $Ca(OH)_2$ to precipitate 3800 t/y of solid waste, characterized as 28 %wt $CaCO_3{\cdot}2H_2O$ and 72 %wt. $CaSO_4{\cdot}2H_2O$. Following this step, the precipitated waste was filtered out, and the NaOH-enriched solution was recirculated within the recycling process as a buffer solution for the neutralization step in the purification process (Cu, Al and Fe removal) after black mass leaching and cementation.

The total energy consumption, considering both electricity and heat, amounts to 621,397 kWh/y (56,753 kWh/y of electricity and 564,644 kWh/y of heat) in scenario 1 and 651,597 kWh/y (69,928 kWh/y of electricity and 586,889 kWh/y of heat) in scenario 2. The energy consumption for the different steps of the process is detailed in the

Table 2
Characterization of NMC pCAM, obtained from previous co-precipitation stage, $Ni_xMn_yCo_{1-x-y}(OH)_2$. Chemical composition and particle size distribution.

Sample	Ni (%)	Mn (%)	Co (%)	Li (%)	S (%)	d10 (μm)	d50 (μm)	d90 (μm)
Co-precipitation product	36.22	9.84	8.67	0.50	3.76	33,3	228	451

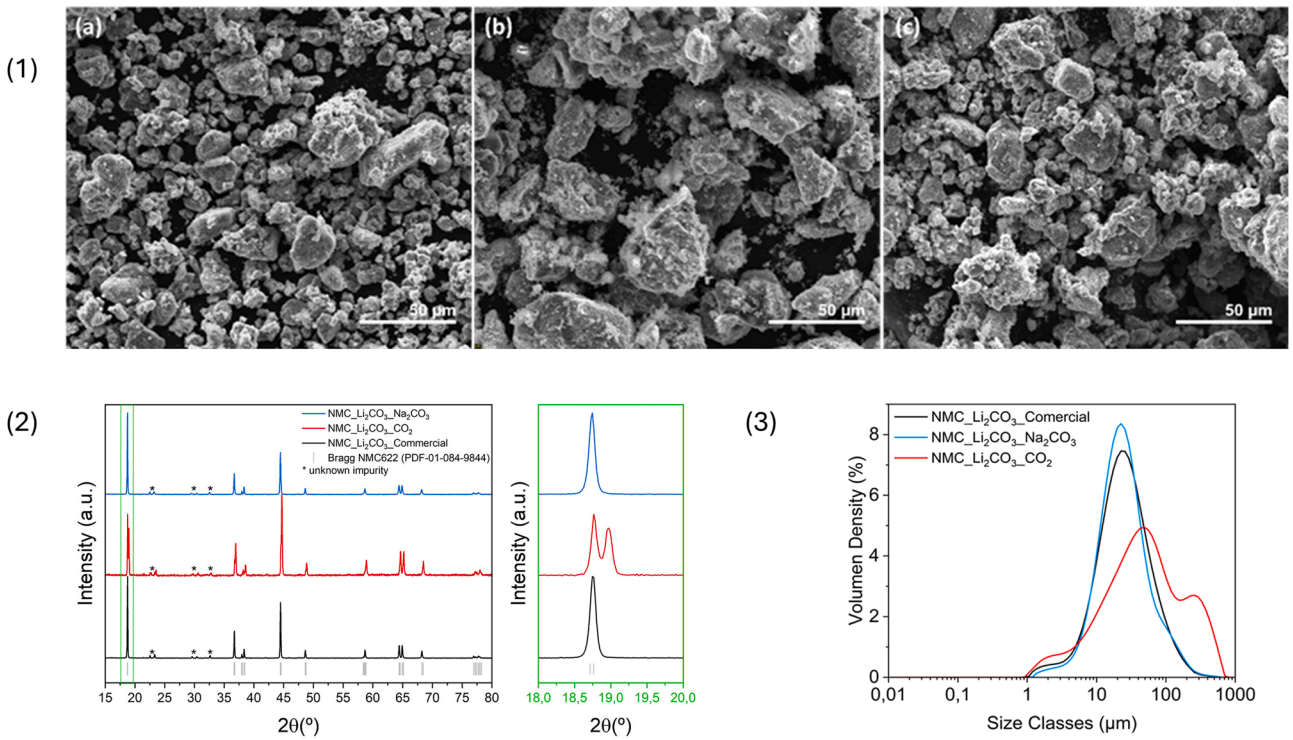

Fig. 4. Morphological and structural characterization of produced NMC622 CAM produced from recycled precursors (1) SEM images of NMC synthesized by co-precipitation and lithiation using (a) Li_2CO_3 recovered by Na_2CO_3 precipitation, (b) Li_2CO_3 recovered by CO_2 bubbling and (c) commercial battery-grade Li_2CO_3. (2) XRD of synthesized NMC622 using different recycled Li_2CO_3 and commercial Li_2CO_3 as precursor. (3) Particle-size distribution of NMC obtained using commercial Li_2CO_3 (blue), Li_2CO_3 precipitated using Na_2CO_3 (green) and Li_2CO_3 precipitated bubbling CO_2 (red).

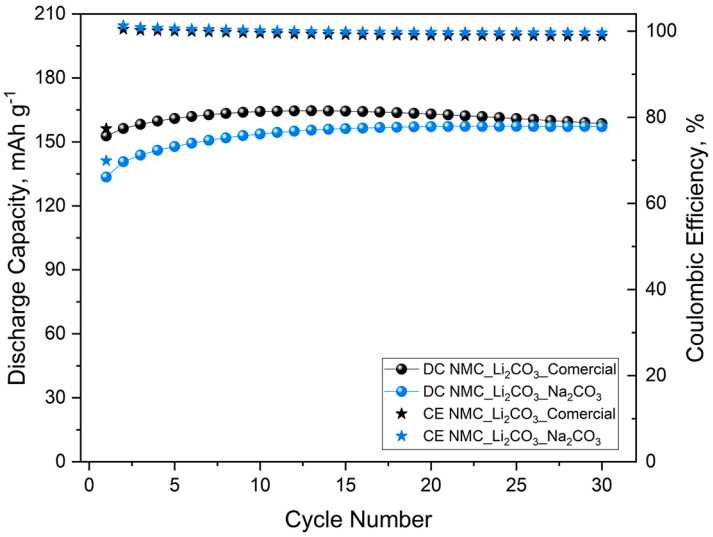

Fig. 5. Cycling performance and coulombic efficiency of NMC622 cathodes obtained from recycled Ni, Mn and Co precursor, commercial Li_2CO_3 and Li_2CO_3 recovered by selective precipitation using Na_2CO_3.

Supplementary Materials Table A2.

3.6. Economic analysis

In Scenario 1, the equipment cost for the recycling facility, including a mixing reactor, heat exchanger, press filter for Li_2CO_3 recovery, and a drum dryer for refining, amounted to 0.67 M€. Including piping, electrical installation, and building infrastructure, the total capital investment reached 1.73 M€. In contrast, Scenario 2 required a more powerful mixing reactor, an additional reactor for preparing the pH buffer solution, and a high-energy ball mill designed for fine grinding and particle size reduction at the micron scale. These additional requirements increased the cost of equipment purchase and installation to 0.87 M€ and the total initial investment to 2.25 M€.

The annual cash flow in each scenario was calculated as the difference between OPEX and revenues from the sale of Li_2CO_3, considering average EU-27 values for electricity and gas price, labour cost and waste management fees and the latest available value of Li_2CO_3 market price. In Scenario 1, revenues from the sale of Li_2CO_3 amounted to 2.03 M€/y, while in scenario 2, revenues increased to 2.56 M€/y, reflecting the

higher recovery rate. OPEX in Scenario 1 were 1.42 M€/y and 1.83 M€/y in Scenario 2. The main cost categories in both scenarios were raw materials (54 % of OPEX in scenario 1 and 42 % of OPEX in Scenario 2) and reagents (22 % of OPEX in Scenario 1 and 34 % of OPEX in Scenario 2). Despite higher OPEX in Scenario 2, the annual cash flow was positive in both, with Scenario 2 yielding +0.73 M€/year and Scenario 1 + 0.62 M€/year, leading to quicker returns: 7 years in Scenario 2 and 9 years in Scenario 1.

A location-based sensitivity analysis across the EU-27 and countries, including Denmark, Sweden, Finland, Germany, Italy, Spain, Poland, and Romania, revealed that both scenarios are economically viable in all regions, though profitability and payback time vary depending on local conditions, see Fig. 6.

Scenario 2 showed a quicker return on investment across all countries, due to the higher revenues, despite higher energy consumption due to the additional processing steps, such as mixing the pH buffer solution and ball milling the recovered Li_2CO_3. Energy and labour costs are key profitability drivers, with energy costs playing a more significant role in Scenario 2, due to the extra steps involved. Countries with higher energy prices, such as Denmark and Sweden, face higher OPEX making them less favourable locations, while Romania stands out as a more cost-effective option, benefiting from lower energy costs. In general, Scenario 1, with lower energy demand, is more stable and suitable for regions with moderate energy costs.

The market-based sensitivity analysis illustrates how fluctuations in the price of Li_2CO_3 directly influence the economic profitability of the two scenarios, see Supplementary Materials Table S3. In 2022, when the market price peaked at 35,677 €/t, the revenues for Scenario 1 were 5.86 M€/y, and for Scenario 2, they were 7.33 M€/y, resulting in a 100 % ROI just 1 year for both scenarios. In contrast, in 2020, when the price dropped to 7283 €/t, Scenario 1 generated 684,600 €/y in revenue, with a payback time extending beyond 20 years, and Scenario 2 generated only 40,331 €/y, with a payback period also extending beyond 20 years. Therefore, Scenario 2 benefits more from price increases, as seen in 2022, where higher revenues from better recovery and purity significantly improve its profitability. However, Scenario 1 remains more stable under market fluctuations and is more resilient to downturns, making it a safer option during low-price years like 2020. The threshold market price for Li_2CO_3 to ensure a positive cash flow is 6947 €/t in Scenario 1 and 7126 €/t in Scenario 2. However, higher thresholds are required for achieving a 100 % ROI after 20 years, corresponding to 8884 €/t in Scenario 1 and 8711 €/t in Scenario 2. This difference is due to the additional revenues generated by the enhanced product recovery in Scenario 2, which makes it economically feasible at a slightly lower price compared to Scenario 1.

Alongside the market-based sensitivity analysis, profits from recovering 1 t of Li_2CO_3 were calculated for both scenarios using EU-27 benchmarks. Scenario 1 yields €2992/t, while Scenario 2 generates €2846/t. The lower profit in Scenario 2 results from higher operational costs, which offset the benefits of improved recovery and product purity. In conclusion, while Scenario 2 offers higher profitability and a quicker return on investment, it is more sensitive to energy price fluctuations and is best suited for regions with low energy costs, whereas Scenario 1, although less profitable, is more stable and remains viable across a broader range of market conditions, making it a safer option during low-price year.

3.7. Environmental analysis

The environmental analysis performed in this study is based on the comparison between the GHG emissions generated and avoided by Li_2CO_3 recycling, in the two scenarios. The emissions factors affecting the environmental impact of recycling were clustered into three categories: energy consumption (considering electricity and heat), reagents (including Na_2CO_3 for scenario 1 and CO_2, NaOH and water for Scenario 2, $Ca(OH)_2$ for both scenarios) and waste management. Besides in this analysis, an additional factor was included to reflect the environmental benefits of Li_2CO_3 recycling compared to primary extraction. Indeed, the emissions associated with extraction activities were considered as a negative contribution to the net GHG emissions balance. Considering the average EU-27 data, the GHGs emissions generated amounts to 2468 t CO_2 eq./y in Scenario 1 and 5234 t CO_2 eq./y in Scenario 2. The higher amount of GHG emissions generated in Scenario 2 are caused by the increased energy consumption and reagent use, primarily due to the

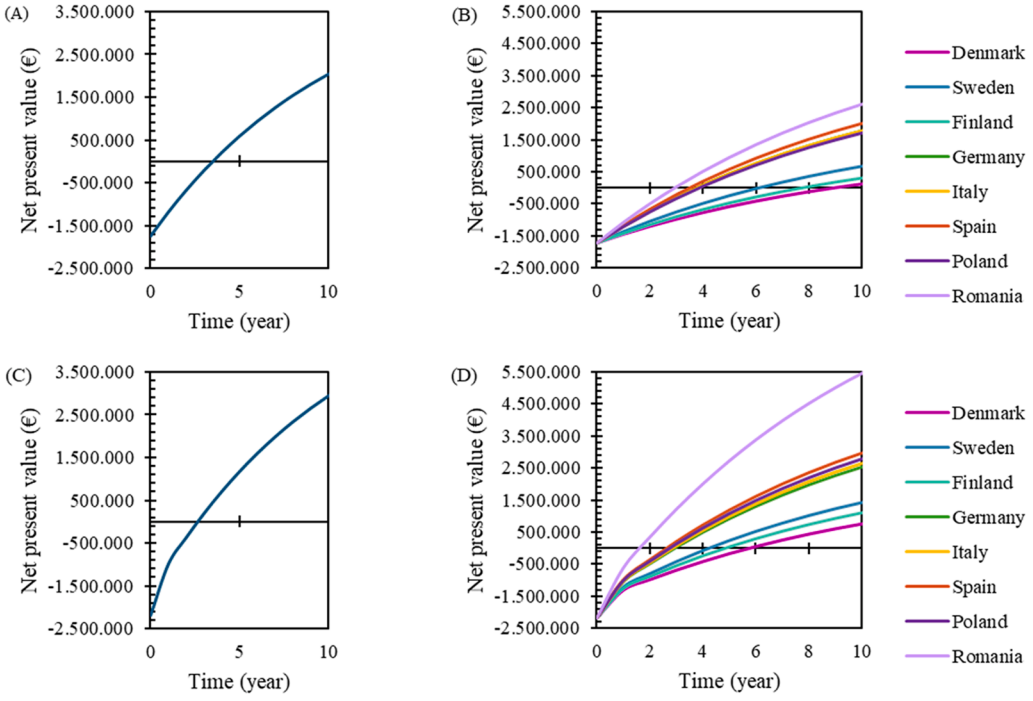

Fig. 6. Net present value (M€) over time for Li_2CO_3 recovery, according to (A) Scenario 1 (chemical precipitation of Li_2CO_3 by addition of Na_2CO_3) in the EU-27 and (B) different European countries, (C) Scenario 2 (recovery of Li_2CO_3 via CO_2 flow) in the EU-27, and (D) different European countries.

additional steps involved in the process. Nonetheless, both scenarios show a net reduction in GHG emissions, corresponding to −518 t CO_2 eq./y in Scenario 1 and −985 t CO_2 eq./y. Scenario 2 represents a more environmentally effective solution since it leads to a higher overall reduction in GHGs emissions, due to the contribution of the avoided emissions from the increased yield of Li_2CO_3 recovery. The environmental analysis was extended to assess net GHG emissions from recovering 1 t of Li_2CO_3. Scenario 1 results in −2479 kg CO_2/t, while Scenario 2 achieves a greater reduction of −3846 kg CO_2/t, showing higher GHG avoidance per unit recovered. This is mainly due to Scenario 2's higher yield, which offsets its increased energy and reagent use.

The environmental sensitivity analysis focuses on the GHG emissions generated and avoided during the Li_2CO_3 recovery process across different European countries. The analysis examines the impact of energy consumption, the use of reagents, and waste management practices on GHG emissions. The resulting GHG emissions balance in EU-27 and in different countries is shown in Fig. 7.

The geographic variability in GHG emissions is strongly influenced by each country's energy mix and waste management practices. For example, Denmark and Sweden, which have a higher share of renewable energy sources, experience lower GHG emissions compared to countries like Poland and Romania, which rely more heavily on fossil fuels for electricity generation. In Scenario 1, the GHG generated in Denmark are 3030 t CO_2/y, while the avoided emissions are 3610 t CO_2/y, resulting in a net reduction of 585 t CO_2/y. This is due to Denmark's cleaner energy mix, which reduces the emissions associated with energy consumption. On the other hand, Poland generates 3330 t CO_2/y of GHG in Scenario 1, with avoided emissions of 3610 t CO_2/y, leading to a net reduction of 285 t CO_2/y. However, the carbon intensity of Poland's energy mix increases the generated GHG, making the environmental benefits of Li_2CO_3 recovery less significant compared to countries with more sustainable energy sources.

In Scenario 2, the energy consumption is higher due to additional processing steps, leading to a greater environmental impact. In Denmark, the GHG emissions generated in Scenario 2 are 3490 t CO_2/y, with 4550 t CO_2/y avoided, resulting in a net reduction of 1060 t CO_2/y. The cleaner energy mix in Denmark allows for a more significant reduction in GHG, as the emissions from energy use are lower. In Poland, however, Scenario 2 generates 3810 t CO_2/y in GHG, with 4550 t CO_2/y avoided, resulting in a smaller net reduction of 739 t CO_2/y. The higher reliance on fossil fuels in Poland increases the GHG emissions generated during the process, reducing the overall environmental benefit of Scenario 2.

Overall, Scenario 2 results in a larger net reduction in GHG emissions across the EU-27, with a net reduction of 986 t CO_2/y, compared to 518 t CO_2/y in Scenario 1. However, Scenario 2 is more dependent on the energy mix, with countries using lower-carbon sources showing the greatest environmental benefits. In contrast, Scenario 1 is better suited for regions with higher carbon intensity, as the impact of increased energy use is less significant in terms of overall GHG emissions. Improving energy mixes and enhancing waste management would yield notable environmental benefits for both scenarios, especially in fossil fuel–reliant countries.

A comparative analysis was conducted to assess how geographic context influences the economic viability and environmental sustainability of the proposed recycling process (Fig. 7). Scenario 2 consistently delivers higher avoided GHG emissions than Scenario 1 across all countries. A clear trade-off emerges: Romania provides the highest economic return, especially in Scenario 2, while Denmark and Sweden are most favorable for minimizing environmental impact. Germany, Italy, and Spain offer a balanced compromise with moderate cash flow and relatively high avoided emissions. In contrast, Poland shows strong economic potential but the lowest avoided emissions, making it less attractive for sustainability-focused objectives. Ultimately, plant location depends on whether economic return or environmental performance is prioritized in meeting Europe's Li demand.

4. Conclusions

This study presents a closed-loop hydrometallurgical recycling strategy that integrates optimized Li recovery and wastewater treatment to directly produce recycled NMC CAM from black mass, promoting

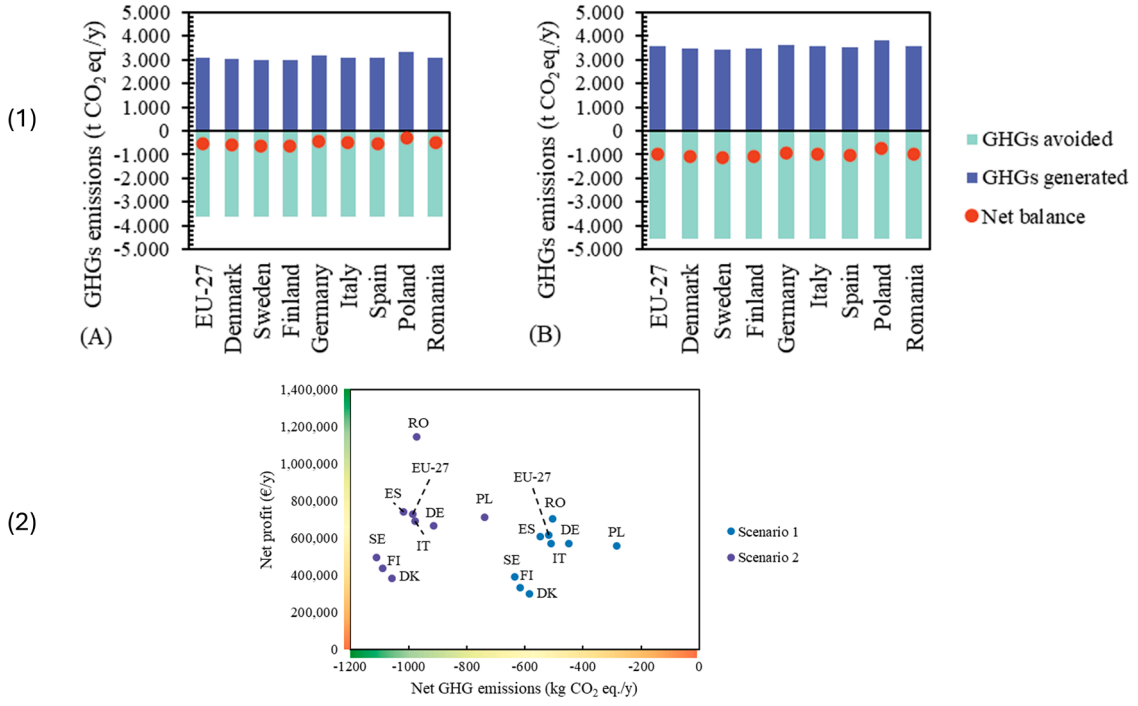

Fig. 7. (1) Net balance of GHG emissions generated and avoided during Li_2CO_3 recovery according to (A) Scenario 1 (chemical precipitation of Li_2CO_3 by addition of Na_2CO_3) and (B) Scenario 2 (recovery of Li_2CO_3 via CO_2 flow). (2) Trade-off analysis between net cashflow and net GHG emissions for scenario 1 and scenario 2 across the selected countries.

circularity in battery manufacturing:

- Li_2CO_3 Recovery Methods:
  - Homogeneous (Na_2CO_3): 77.8 % recovery at >97 % purity.
  - Heterogeneous (CO_2): 97.1 % recovery at >97 % purity.
  - Trade-off observed: longer residence times for heterogeneous precipitation increase particle size, requiring post-milling (d_{80} = 36.6 μm) to meet battery-grade specifications.
- Electrochemical Performance:
  - Recycled Li_2CO_3-based NMC cathodes performed comparably to commercial ones.
  - Commercial Li_2CO_3-based cathode stabilized at 161 $mAh.g^{-1}$ after 30 cycles, while the recycled counterpart reached 157 $mAh.g^{-1}$, both achieving ~100 % coulombic efficiency.
- Techno-Economic Assessment:
  - Scenario 2: Delivers higher profitability and faster ROI (1 year at €35,677/t in 2022) but is best suited to regions with low energy costs due to greater sensitivity to energy price fluctuations.
  - Scenario 1: Provides a more stable ROI and lower sensitivity to energy costs, making it suitable for regions with moderate prices and still viable in low-price years like 2020, with ROI exceeding 20 years at €7283/t.
- Environmental Impact:
  - Both scenarios reduce GHG emissions: Scenario 2 achieves greater reductions in countries with clean energy, while Scenario 1 is more effective in regions with high carbon intensity.

Heterogeneous precipitation combined with tailored micronization offers superior economic and environmental benefits compared to direct homogeneous precipitation. However, it is more sensitive to energy price volatility and the share of renewable energy.

CRediT authorship contribution statement

Néstor Antuñano: Writing – review & editing, Writing – original draft, Validation, Supervision, Methodology, Investigation, Formal analysis, Data curation, Conceptualization. **Marlo Angelo Tito:** Writing – review & editing, Writing – original draft, Methodology, Investigation, Formal analysis, Data curation, Conceptualization. **Cristina Balza de Vallejo:** Writing – review & editing, Writing – original draft, Methodology, Investigation, Formal analysis, Data curation, Conceptualization. **Montserrat Galcerán:** Writing – review & editing, Writing – original draft, Validation, Formal analysis, Data curation. **Martina Bruno:** Writing – review & editing, Writing – original draft, Methodology, Formal analysis, Data curation. **Silvia Fiore:** Writing – review & editing, Writing – original draft, Validation, Supervision, Conceptualization.

Declaration of competing interest

The authors declare that they have no known competing financial interests or personal relationships that could have appeared to influence the work reported in this paper.

Acknowledgments

This work was supported by funding from the Basque Government through the **ELKARTEK CICe2025** program (ref. KK2025-00054)

Supplementary materials

Supplementary material associated with this article can be found, in the online version, at doi:10.1016/j.rcradv.2025.200291.

Data availability

Data will be made available on request.

References

Aprilianto, D.R., et al., 2024. Effect of sulfate and carbonate ions on lithium carbonate precipitation from a low concentration lithium containing solution. Ind. Eng. Chem. Res. 63, 4918–4933. https://doi.org/10.1021/acs.iecr.3c04294.
Bataglia, G., et al., 2022. Recovery of lithium carbonate from dilute Li-rich brine via homogenous and heterogeneous precipitation. Ind. Eng. Chem. Res. 61 (36), 13589–13602. https://doi.org/10.1021/acs.iecr.2c01397.
Benchmark Mineral Intelligence, 2025. Lithium prices, data & market analysis [WWW Document]. URL. https://www.benchmarkminerals.com/lithium/lithium-prices/chart (accessed 1.22.25).
Bruno, M., Fiore, S., 2024. Review of lithium-ion batteries' supply-chain in Europe: material flow analysis and environmental assessment. J. Environ. Manage 358, 120758. https://doi.org/10.1016/j.jenvman.2024.120758.
Chang, H.F., et al., 2025. Advanced absolute chemical precipitation for high-purity metal recovery in all-types of lithium-ion battery recycling. Sep. Purif. Technol. 361. https://doi.org/10.1016/j.seppur.2025.131454.
Chemical Engineering Projects, 2014. Estimation of purchased equipment costs [WWW Document]. URL. https://chemicalprojects.wordpress.com/category/design-and-simulation/ (accessed 12.12.24).
Degen, F., et al., 2023. Energy consumption of current and future production of lithium-ion and post lithium-ion battery cells. Nat. Energy 8, 1284–1295. https://doi.org/10.1038/s41560-023-01355-z.
Ecoinvent, 2024. ecoinvent Version 3.9 [WWW Document]. URL. https://support.ecoinvent.org/ecoinvent-version-3.8 (accessed 10.21.24).
European Environment Agency, 2024. Greenhouse gas emission intensity of electricity generation in Europe [WWW Document]. URL. https://www.eea.europa.eu/en/analysis/indicators/greenhouse-gas-emission-intensity-of-1 (accessed 12.13.24).
European Environmental Agency, 2023. Technical note accompanying the EEA briefing "economic instruments and separate collection-key instruments to increase recycling.".
European Union, 2023. REGULATION (EU) 2023/1542 OF THE EUROPEAN PARLIAMENT AND OF THE COUNCIL of 12 July 2023 concerning batteries and waste batteries, amending Directive 2008/98/EC and Regulation (EU) 2019/1020 and repealing Directive 2006/66/EC.
Eurostat, 2024a. Electricity prices for non-household consumers - bi-annual data (from 2007 onwards) [WWW Document]. URL. https://ec.europa.eu/eurostat/databrowser/view/nrg_pc_205/default/table?lang=en&category=nrg.nrg_price.nrg_pc (accessed 7.29.24).
Eurostat, 2024b. Gas prices for non-household consumers - bi-annual data (from 2007 onwards) [WWW Document]. URL. https://ec.europa.eu/eurostat/databrowser/view/nrg_pc_203/default/table?lang=en (accessed 11.26.24).
Eurostat, 2024c. Labour cost for LCI (compensation of employees plus taxes minus subsidies) [WWW Document]. URL. https://ec.europa.eu/eurostat/databrowser/view/lc_lci_lev_custom_13925961/default/table?lang=en (accessed 11.26.24).
Franke, J., Mersmann, A., 1995. The influence of the operational conditions on the precipitation process. Chem. Eng. Sci. 50 (11), 1737–1753. https://doi.org/10.1016/0009-2509(95)00028-4.
Gaines, L., et al., 2023. Tracking flows of end-of-life battery materials and manufacturing scrap. Batteries. (Basel) 9 (7), 360. https://doi.org/10.3390/batteries9070360.
Gao, W., et al., 2018. Selective recovery of valuable metals from spent lithium-ion batteries – Process development and kinetics evaluation. J. Clean. Prod. 178, 833–845. https://doi.org/10.1016/j.jclepro.2018.01.040.
Garole, D.J., et al., 2020. Recycle, recover and repurpose strategy of spent Li-ion batteries and catalysts: current status and future opportunities. ChemSusChem. 13 (12), 3079–3100. https://doi.org/10.1002/cssc.201903213.
Gu, K., et al., 2024. The factors influencing lithium carbonate crystallization in spent lithium-ion battery leachate. Processes 12. https://doi.org/10.3390/pr12040753.
Han, B., et al., 2020a. Lithium carbonate precipitation by homogeneous and heterogeneous reactive crystallization. Hydrometallurgy 195. https://doi.org/10.1016/j.hydromet.2020.105386.
Han, X., et al., 2020b. A full battery system of pre-lithiated phosphorus/sulfurized pyrolyzed poly(acrylonitrile) with an effective electrolyte and improved safety. Green Chemistry 22, 4252–4258. https://doi.org/10.1039/d0gc01173h.
Hool, A., et al., 2023. Challenges and opportunities of the European Critical Raw Materials Act. Min. Econ. 37, 661–668. https://doi.org/10.1007/s13563-023-00394-y.
Idemoto, Y., et al., 1997. Crystal structure of (LixK1 − x)2CO3 (x = 0, 0.43, 0.5, 0.62, 1) by neutron powder diffraction analysis. J. Phys. Chem. SolidsVol. 59 (3), 363–376. https://doi.org/10.1016/S0022-3697(97)00209-6.
Jose, S.A., et al., 2024. Critical review of lithium recovery methods: advancements, challenges, and future directions. Processes (10), 12. https://doi.org/10.3390/pr12102203.
Joshi, B., et al., 2024. Selective lithium recovery from pyrolyzed black mass through optimized caustic leaching. J. Environ. Chem. Eng. 12. https://doi.org/10.1016/j.jece.2024.113787.
Joshi, B., et al., 2025. Optimizing lithium carbonate recovery through gas-liquid reactive crystallization of lithium hydroxide and carbon dioxide. Sustain. Mater. Technol. 44. https://doi.org/10.1016/j.susmat.2025.e01341.
Kim, S.H., et al., 2024. Carbon dioxide utilization in lithium carbonate precipitation: a short review. Environ. Eng. Res. 29 (3). https://doi.org/10.4491/eer.2023.553.
Larouche, F., et al., 2020. Progress and status of hydrometallurgical and direct recycling of Li-ion batteries and beyond. Materials. (Basel) 13 (3), 801. https://doi.org/10.3390/ma13030801.

Latini, D., et al., 2022. A comprehensive review and classification of unit operations with assessment of outputs quality in lithium-ion battery recycling. J. Power. Sources. 546, 231979. https://doi.org/10.1016/j.jpowsour.2022.231979.
Lewis, A., et al., 2015. Industrial Crystallization: Fundamentals and Applications. Cambridge University Press, Cambridge, UK.
Liu, C., et al., 2019. Recycling of spent lithium-ion batteries in view of lithium recovery: a critical review. J. Clean. Prod. 228, 801–813. https://doi.org/10.1016/j.jclepro.2019.04.304.
Loh, H.P., et al., 2002. Process equipment cost estimation final report.
Marcinov, V., et al., 2023. Lithium production and recovery methods: overview of Lithium losses. Metals. *Metals (Basel)* 13, 1213. https://doi.org/10.3390/met13071213.
Melchor-Martínez, E.M., et al., 2021. Environmental impact of emerging contaminants from battery waste: a mini review. Case Studies Chem. Environ. Eng. 3. https://doi.org/10.1016/j.cscee.2021.100104.
Mrozik, W., et al., 2021. Environmental impacts, pollution sources and pathways of spent lithium-ion batteries. Energy Environ. Sci. 14, 6099–6121. https://doi.org/10.1039/d1ee00691f.
Qing, J., et al., 2023. Novel approach to recycling of valuable metals from spent lithium-ion batteries using hydrometallurgy, focused on preferential extraction of lithium. J. Clean. Prod. 431. https://doi.org/10.1016/j.jclepro.2023.139645.
Raiguel, S., et al., 2023. Recovery of lithium from simulated nanofiltration-treated seawater desalination brine using solvent extraction and selective precipitation. Solvent Extract. Ion Exchange 41, 425–448. https://doi.org/10.1080/07366299.2023.2206440.
Ramírez Velázquez, L.E., et al., 2024. Recovery of lithium from Li-ion battery leachate by gas-liquid precipitation. J. Cryst. Growth 631. https://doi.org/10.1016/j.jcrysgro.2024.127625.
Rodriguez-Carvajal, J., 1993. Recent advances in magnetic structure determination by neutron powder diffraction. Phys. B: Condensed Matter 192 (1–2), 55–69. https://doi.org/10.1016/0921-4526(93)90108-I.
Tahmasebi, M.H., Obrovac, M.N., 2024. New insights into the all-dry synthesis of NMC622 cathodes using a single-phase rock salt oxide precursor. ACS. Omega 9, 1916–1924. https://doi.org/10.1021/acsomega.3c08702.
Titirici, M., et al., 2024. 2024 roadmap for sustainable batteries. J. Phys.: Energy 6 (4). https://doi.org/10.1088/2515-7655/ad6bc0.
US Inflation Calculator, 2025. Inflation calculator | find US dollar's value from 1913 to 2025 [WWW Document]. URL. https://www.usinflationcalculator.com/ (accessed 1.22.25).
Velázquez-Martínez, O., et al., 2019. A critical review of lithium-ion battery recycling processes from a circular economy perspective. Batteries. (Basel) 5 (4), 68. https://doi.org/10.3390/batteries5040068.
Wylock, C., et al., 2014. Analysis of the simultaneous gas–Liquid CO2 absorption and liquid–Gas NH3 desorption in a hydrometallurgical waelz oxides purification process". Int. J. Chem. Reactor Eng. 12 (1), 549–562. https://doi.org/10.1515/ijcre-2014-0034.
Yu, L., et al., 2023. Efficient separation and coprecipitation for simplified cathode recycling. Energy Storage Mater. 63, 103025. https://doi.org/10.1016/j.ensm.2023.103025.
Zhao, T., et al., 2019. The role of precipitant in the preparation of lithium-rich manganese-based cathode materials. Chem. Phys. Lett. 730, 354–360. https://doi.org/10.1016/j.cplett.2019.06.034.
Zhao, Z., et al., 2025. Multistage gradient crystallization study towards lithium carbonate crystal growth. Sep. Purif. Technol. 360. https://doi.org/10.1016/j.seppur.2024.130955.